PAPER

Synthesis and characterization of uniform OCL-OEG block cooligomers†

Philipp Bohn,[a] Valerian Hirschberg,[b] Simon Buchheiser,[c] Dafni Moatsou, [ID][d] Hermann Nirschl[c] and Michael A. R. Meier [ID] *[a,d]

Block copolymers are an interesting class of materials, offering the opportunity to form nanostructured morphologies, making them suitable for a broad range of applications in nanotechnology, medicine, or biotechnology. Especially for the pharmaceutical sector, a uniform structure and a distinct structure–property relationship is desirable to manufacture highly reproducible and tailor-made materials. Herein, we report the synthesis and characterization of uniform ($Đ$ = 1.01) oligo(ε-caprolactone)-oligo(ethylene glycol) (OCL-OEG) block co-oligomers (BCOs). Three different BCOs, varying in the length of the hydrophobic caprolactone segment, were obtained *via* Steglich esterification of the corresponding homo oligomers. A clear dispersity and composition dependent structure–property relationship based on the thermal properties is observed, compared to identical structures similar in M_n and dispersities of $Đ$ = 1.06, obtained *via* ring-opening polymerization (ROP) of ε-caprolactone. In addition, increased long-range-order distances L_0 with increasing dispersity of the BCOs are found for the formed morphologies after solvent vapor annealing (SVA). These results highlight the importance of uniform structures for a better understanding of the structure–property relationship of block copolymers.

Introduction

Inspired by the highly defined structures of biomacromolecules (*e.g.* DNA, RNA or proteins), which exhibit architectures of synthetically unreached complexity and thus enable complex natural processes, current research in polymer chemistry focuses on the synthesis of uniform and sequence-defined macromolecules. Especially block copolymers (BCP)s are of interest due to their self-assembly (SA) capability,[1,2] which is the basis for several applications including drug delivery,[3] organic optoelectronics,[4] or as supramolecular materials for membranes.[5] The experimental SA of copolymers, supported by theoretical studies such as the Flory–Huggins theory[6] or the self-consistent mean field theory (SCMFT),[7] has been extensively investigated since the 1960s for the SA in

bulk[2,8] and in solution.[9] In bulk, the SA of a diblock copolymers (A_nB_m) depends on the Flory–Huggins Parameter, χ_{AB}, describing the energy of the thermodynamic immiscibility normalized to k_bT of the two homoblocks A and B, the degree of polymerization, N, and the volume fractions of block A (Φ_A) and block B (Φ_B). More recently, the tuneability and predictability of the formed morphologies, depending on the dispersity[10,11,12–15] and the shape of the molecular weight distribution,[16–18] have gained interest in polymer chemistry and nanotechnology.

However, since the field of polymer chemistry has always been the science of molecular weight distribution and structural dispersity, the synthesis of perfectly defined structures, as present in some biopolymers in nature, remained an unreached goal for a long time.[19] In the last decade, progress in the preparation of tailor-made materials was described by controlling the monomer sequence and molecular weight distribution down to uniformity[18,20] and insights into the distinct structure–property relationship of macromolecules became accessible. Thus, these structures made a significant contribution to material and life science.[21,22]

Pioneering work for the synthesis of uniform and sequence-defined structures has been set by Robert B. Merrifield with the development of the Solid-Phase-Peptide-Synthesis (SPPS) in 1963,[23] for which he was awarded the 1984 Nobel Prize.[24] The concept was transferred to other classes of polymers, such as peptoids,[25] glycopeptides,[26] or oligonucleo-

[a]Laboratory of Applied Chemistry, Institute of Organic Chemistry (IOC), Karlsruhe Institute of Technology (KIT), Straße am Forum 7, 76131 Karlsruhe, Germany. E-mail: m.a.r.meier@kit.edu; https://www.meier-michael.com
[b]Institute of Chemical Technology and Polymer Chemistry (ITCP), Karlsruhe Institute of Technology (KIT), Engesserstraße 18, 76131 Karlsruhe, Germany
[c]Institute for Mechanical Process Engineering and Mechanics (MVM), Karlsruhe Institute of Technology (KIT), Straße am Forum 8, 76131 Karlsruhe, Germany
[d]Laboratory of Applied Chemistry, Institute of Biological and Chemical Systems – Functional Molecular Systems (IBCS-FMS), Karlsruhe Institute of Technology (KIT), Eggenstein-Leopoldshafen, 76344 Germany
†Electronic supplementary information (ESI) available. See DOI: https://doi.org/10.1039/d3py01052j

tides,[27] and has set the foundation for an enormous variety of synthetic sequence-defined macromolecules.[22,28] Furthermore, different approaches, including solid-[29] and liquid phase,[30] or solid supported synthesis,[31] single unit monomer insertion (SUMI),[32] or template assisted synthesis were investigated.[33] In this context, the iterative exponential growth (IEG) strategy was developed, allowing a fast build-up of uniform macromolecules.[34]

The first studies using an iterative synthesis protocol towards uniform block copolymers was reported by Meijer *et al.* in 2016.[12] The obtained dimethylsiloxane (DMS)-lactic acid BCOs up to the dononacontamer showed distinct order–disorder transitions and were compared to narrowly distributed analogues. An increase in domain spacing and surprising stability of the morphology (increase of T_{ODT}), and a decrease of the overall degree of ordering with increasing dispersity was observed.[13] The same group has shown the temperature-controlled formation of 1D and 2D nanostructures of hydrazone-*o*DMS di- and triblockcooligomers.[35] The mixing of these discrete BCOs, the tuneability of the phase behavior for blends with $Đ ≤ 1.10$, as well as the difference to a disperse sample was recently investigated by Fors and Meijer. Furthermore, microphase segregation was observed for disperse oligomer mixtures containing more than 50 mol% of the discrete compound similar in length and volume fraction, underlining the differences of discrete and disperse BCOs.[36] In 2020, the group of Hawker demonstrated an efficient and rapid preparation of discrete diblock copolymer libraries using automated chromatographic fractionation of a single narrowly distributed poly(dodecyl acrylate)-*block*-poly(lactide) (PDDA-*b*-PLA).[14] This technique simplifies the investigations of the phase behavior, and allows insights into new morphologies of novel BCPs. Using the same strategy, oligo(3-hexylthiophene), which showed a distinct crystallization behavior and optical properties, dependent on chain length,[37] were described. Moreover, lipid monodisperse PEG derivatives showed a reduced anti-PEG antibody recognition compared to molecular weight disperse analogues.[38] The same group demonstrated the application of this method to triblock terpolymers. The purified samples showed an increase in long-range order compared to the parent polymers.[39] The stereochemical effect in uniform PLA-PEG BCPs were reported by Kim *et al.* in 2021. Irregular nanostructures were observed for complementary configured monodisperse poly(lactic acid), whereas triangular and vascular nanostructures were formed for mismatched or stereochemical sequences.[40]

Here, we report the synthesis of uniform ($Đ = 1.01$) as well as narrowly distributed ($Đ = 1.06$) oligo(ε-caprolactone)-oligo(ethylene glycol) (OCL-OEG) block *co*-oligomers (BCOs), obtained *via* an iterative exponential approach or ring-opening polymerization, respectively. The PEG-PCL system is of special interest due to its biocompatibility, biodegradability, and application in the pharmaceutical sector as drug delivery systems, where a distinct structure–property relationship and the control of it *via* chemical reactions is crucial. We aimed for three comparable BCO pairs, varying in the length of the
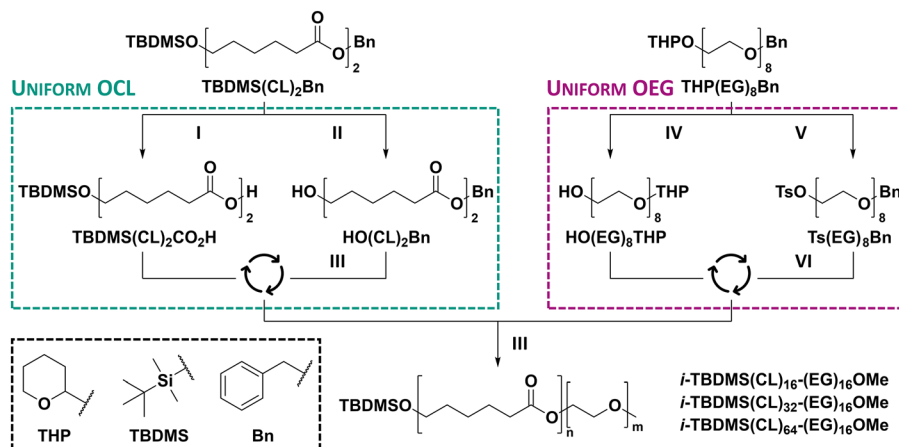
hydrophobic caprolactone block (mOEG$_n$-*b*-OCL$_m$-TBDMS; $n = 16$, $m = 16, 32, 64$; $Φ_{OCL} = 0.71–0.92$) to investigate their dispersity and constitution dependent structure–property relationship. Comparison of the thermal properties and shifts in the long-range-order distances highlight the difference of uniform and narrowly distributed ($Đ = 1.06$), often incorrectly labeled as monodisperse, macromolecules.

Results and discussion

OEG-OCL block cooligomers were synthesized *via* coupling of the monoprotected homooligomers (Scheme 1), which were obtained using an iterative exponential growth strategy. The caprolactone oligomer was prepared according to the procedure of Hawker *et al.* performing first a base-catalyzed nucleophilic ring opening of ε-caprolactone to obtain the starting monomer, 6-hydroxycaproic acid, **HO(CL)$_1$CO$_2$H**.[41] Half of the sample was protected using a *tert*-butyldimethylsilyl (TBDMS) ether as protecting group of the alcohol and the other half using a benzyl ester for the carboxylic acid. The orthogonally protected building units **TBDMS(CL)$_1$CO$_2$H** and **HO(CL)$_1$Bn** were coupled *via* a Steglich esterification using *N,N′*-dicyclohexylcarbodiimide (DCC) and 4-(dimethylamino)pyridine (DMAP) up to the tetramer, **TBDMS(CL)$_4$Bn** and 4-(dimethylamino)pyridinium *p*-toluene sulfonate (DPTS) from the octamer on to suppress the reported side reaction towards the unreactive *N*-acylurea. Afterwards, the sample of the doubly protected tetramer was split, and the protecting groups were cleaved orthogonally. The benzyl ester was deprotected *via* reductive hydrogenation, affording the carboxylic acid, and the silyl ether was deprotected by treatment with tetra-*n*-butyl ammonium fluoride (TBAF) under acidic conditions to yield the desired alcohol. By repetition of the iterative reaction cycle (Scheme 1), consisting of a coupling step and subsequent separate deprotection, an oligo caprolactone containing 64 repeating units was obtained in 20 steps in an overall yield of 33.1%, always considering the lowest yield of the divergent step. The general reaction scheme for the synthesis of uniform polycaprolactone is shown in Scheme 1.

Each of the individual products was characterized by ^{1}H, ^{13}C, and IR spectroscopy, as well as MS (Mass Spectrometry) and SEC to confirm their high purity (≥99% SEC purity). The analytical data are provided in the ESI.† Further, the scale, yield, dispersity, and purity (determined by SEC) are summarized in ESI Table 13.† In accordance to the description of Hawker *et al.*,[41] minor impurities that match to the precursor molecules in terms of respective retention times were observed from the synthesis of the hexadecamer on. Therefore, we focused on the purification of the respective compounds *via* fractionating column chromatography. As an example, a 15.5 mmol (31.8 g) batch of **TBDMS(CL)$_{16}$Bn** was applied on a silica column and eluted as slowly as possible to remove impurities with almost similar retention times. Three of these fractionating isolation steps were performed successively, and in total 46 fractions were collected, 31 of which contained the

Scheme 1 Reaction scheme for the synthesis of uniform OCL-OEG BCOs (*i*-TBDMS(CL)$_n$-(EG)$_{16}$OMe (n = 16, 32, 64)) from the corresponding OCL and OEG homooligomers, which were obtained *via* an iterative exponential growth strategy; green iteration cycle:[41] I: hydrogenation of benzyl ester with H$_2$, Pd/C, in EA at rt. o.n.; II: TBDMS deprotection with TBAF, AcOH, in THF at 50 °C o.n.; III: Steglich esterification with DCC, DMAP in DCM at rt o.n.; purple iteration cycle: IV: hydrogenation of benzyl ether with H$_2$, Pd/C, in EA at reflux o.n.; V: THP deprotection: *p*-TsOH in MeOH at rt, 36 h; tosylation: NaOH, *p*-TsCl in H$_2$O/THF at rt, 15 h; VI: ether coupling: KO^{t}Bu (potassium *tert*-butoxide) in THF, 0 – rt, o.n.; THP deprotection: *p*-TsOH in MeOH at rt, 36 h; methylation: NaH (sodium hydride), MeI in THF, 0 – rt, o.n.; hydrogenation of benzyl ether with H$_2$, Pd/C, in ethanol at rt o.n.; *i*: prepared *via* an iterative approach..

product in purities ranging from 50.2 to >99% (see ESI† for SEC chromatograms and the evaluated data sets). Only the samples with a SEC-purity of >99% were selected for further synthesis (ESI Tables 7–9,† highlighted in green). It is worthwhile to note that the molecular weight distributions of the unpurified and the purified **TBDMS(CL)$_{16}$Bn** are almost indistinguishable (ESI Fig. 63†), yet the purification was necessary to claim uniformity, as the separated byproducts observed by SEC (ESI Fig. 60–62†) clearly demonstrate.

After extensive comparison of different synthesis protocols to achieve uniform OEGs,[42] a hexadeca(ethylene glycol) **HO(EG)$_{16}$OMe** was prepared (see Scheme 1) according to the procedure of Baker *et al.*[43] and Bruce *et al.*[44] The starting unit, tetra(ethylene glycol), was commercially obtained in a purity of 99%. A benzyl (Bn) ether and a tetrahydropyranyl (THP) ether turned out to be the most efficient orthogonal protecting groups. The THP protection was performed according to a procedure of Baker *et al.*[43] and the product **THP(EG)$_4$OH** was obtained in a yield of 74%, whereas the benzyl group was introduced as described by Bruce *et al.* leading to product **Bn(EG)$_4$OH** (83%).[44] Having installed the orthogonal protecting groups, the next step was the activation of the hydroxyl group of **Bn(EG)$_4$OH** into a tosylate **Bn(EG)$_4$Ts**, thus opening the possibility for an ether coupling of **THP(EG)$_4$OH** and **Bn(EG)$_4$Ts**, and thus a chain doubling. Using NaH as a base, 68% yield of **Bn(EG)$_8$THP** was obtained, whereas KO^{t}Bu resulted in a yield of 48% after purification *via* silica column chromatography (ESI Tables 2 and 3†). A detailed MS study of the occurring side products was described in a previous report and summarized in the ESI Table 1.†[42] Separate deprotection of the orthogonal protecting groups generated the respective unsymmetric alcohols **Bn(EG)$_8$OH** and **THP(EG)$_8$OH** in yields >98%. The THP group was cleaved by treatment with *p*-toluenesulfo-

nic acid in methanol, and the benzyl ether was removed by reductive hydrogenation. By repetition of the tosylation of the benzyl protected species **Bn(EG)$_8$OH**, and a coupling reaction with **THP(EG)$_8$OH**, the double protected hexadecamer **Bn(EG)$_{16}$THP** was obtained. In order to obtain an identical structure for the uniform and the non-uniform BCOs, the protecting group had to be exchanged. Therefore, the THP protected alcohol was cleaved under acidic conditions, resulting in **Bn(EG)$_{16}$OH** in a quantitative yield. Subsequently, a methylation was conducted using methyl iodide in ten-fold excess and NaH as base. Unfortunately, only a decreased yield of 30% of pure product **Bn(EG)$_{16}$OMe** and 70% with a purity of 93–98% were obtained after purification *via* silica column chromatography. In the last step, the benzyl group was deprotected according to a procedure of Haag *et al.*[45] Replacing ethyl acetate with ethanol and conducting the reaction at room temperature instead of reflux, the side reaction was avoided and product **HO(EG)$_{16}$OMe** was obtained in a yield of 98% (overall yield of 3% in 11 steps) and was used without further purification. Full characterization by nuclear magnetic resonance (NMR) and infrared (IR) spectroscopy as well as high resolution-electrospray ionization mass spectrometry (HR-ESI MS) of all oligo (ethylene glycol)s **THP(EG)$_4$OH** – **HO(EG)$_{16}$OMe** and a summary of the SEC chromatograms are provided in the ESI.†

To obtain the desired block cooligomers *i*-TBDMS(CL)$_n$-(EG)$_{16}$OMe (n = 16, 32, 64), the oligocaprolactones **TBDMS(CL)$_n$CO$_2$H** (n = 16, 32, 64) were coupled *via* a Steglich esterification with **HO(EG)$_{16}$OMe** (Scheme 1). Quantitative conversions were achieved by using equimolar amounts of DPTS and 6.00 equiv. of DCC. The formation of the individual products was first confirmed *via* SEC, with the appearance of a new signal at retention times of 15.9 min (*i*-TBDMS(CL)$_{16}$-(EG)$_{16}$OMe), 14.2 min (*i*-TBDMS(CL)$_{32}$-(EG)$_{16}$OMe), and
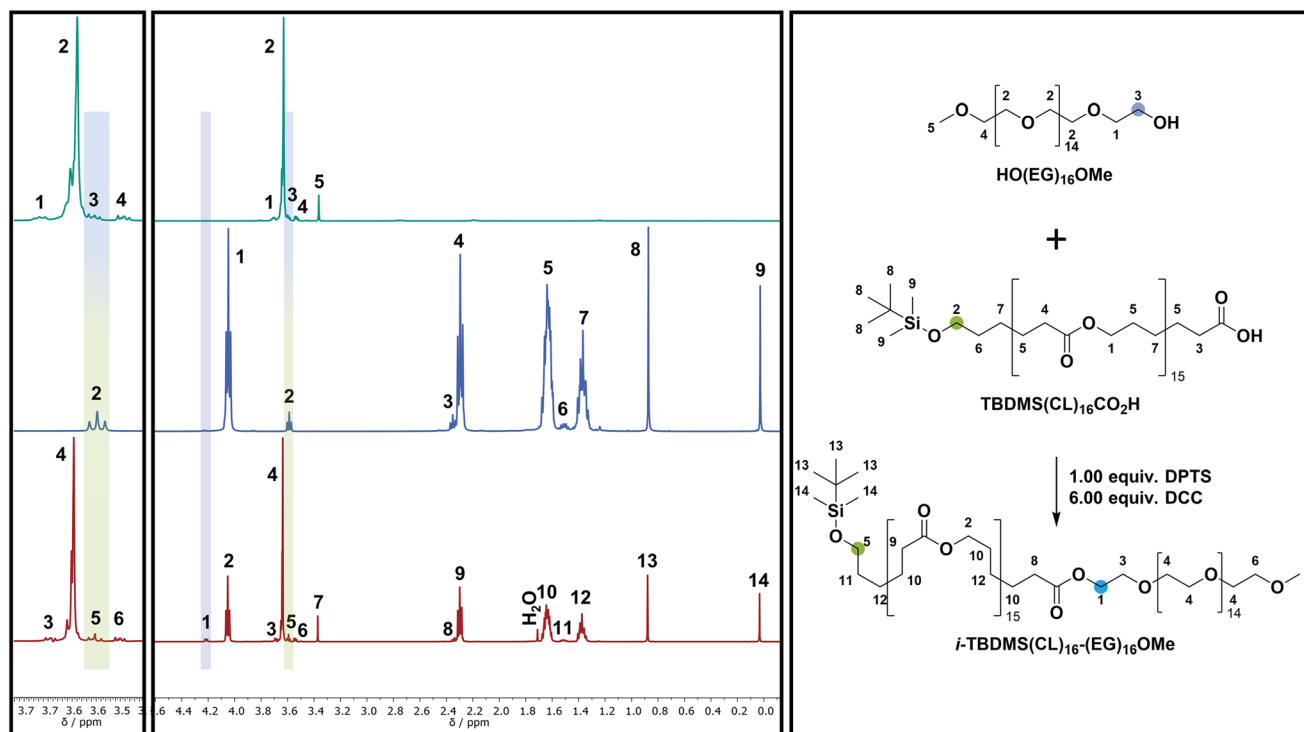
13.2 min (*i*-TBDMS(CL)$_{64}$-(EG)$_{16}$OMe), respectively. For each reaction, separate peaks at earlier retention times indicated the formation of side products of larger hydrodynamic volumes, which were not analyzed further. Similar to the homooligomers, the purification of the three BCOs was challenging *via* silica column chromatography and the products were obtained in yields of 37% (*i*-TBDMS(CL)$_{16}$-(EG)$_{16}$OMe), 43% (*i*-TBDMS(CL)$_{32}$-(EG)$_{16}$OMe) and 18% (*i*-TBDMS(CL)$_{64}$-(EG)$_{16}$OMe), respectively. Purities of >99% and dispersities of *Đ* = 1.01 were determined *via* SEC, respectively. ^{1}H and ^{13}C NMR spectroscopy proved to be helpful to follow the formation of the BCOs. The CH$_2$ signal next to the terminal hydroxyl moiety is shifted upfield from 3.59 to 4.22 ppm in the proton spectrum after esterification (Fig. 1). All other signals remain at the same chemical shift.

COSY and HMBC as well as a comparison of the ^{13}C NMR spectra are provided in the ESI (ESI Fig. 85†) to clarify the peak assignment. DOSY NMR further confirmed the successful coupling reaction (ESI Fig. 86, 97 and 103†). Additionally, HR ESI-MS analysis was performed. The found mass and the experimental isotopic pattern of the single or double charged sodium adducts matched with the calculated *m/z* values (*i*-TBDMS(CL)$_{16}$-(EG)$_{16}$OMe [M + Na]$^+$ *m/z* calc. 2698.6106, detected 2698.6143; *i*-TBDMS(CL)$_{32}$-(EG)$_{16}$OMe [M + Na]$^+$ *m/z* calc. 4523.6999, detected 4523.6934; *i*-TBDMS(CL)$_{64}$-(EG)$_{16}$OMe [M + 2Na]$^{2+}$ *m/z* calc. 4100.9427, detected

4100.9558). Unfortunately, impurities of mOEG$_n$-*b*-OCL$_{m-1}$ species were observed for *i*-TBDMS(CL)$_{32}$-(EG)$_{16}$OMe (relative intensity, $I_{rel.}$(mOEG$_{16}$-*b*-OCL$_{31}$[M + 2Na]$^{2+}$) = 33), and *i*-TBDMS (CL)$_{64}$-(EG)$_{16}$OMe (relative intensity $I_{rel.}$(mOEG$_{16}$-*b*-OCL$_{63}$[M + 3Na]$^{3+}$) = 17, see ESI Fig. 98 and 104†) in the ESI-MS spectra. Therefore, only *i*-TBDMS(CL)$_{16}$-(EG)$_{16}$OMe can be considered as truly uniform with respect to MS analysis, whereas *i*-TBDMS (CL)$_{32}$-(EG)$_{16}$OMe and *i*-TBDMS(CL)$_{64}$-(EG)$_{16}$OMe must be classified as non-uniform according to the definition of IUPAC.[46]

In order to investigate the structure–property relationship in terms of the self-assembly behavior of the amphiphilic block cooligomers, identical structures, similar in M_n with the uniform BCOs, but exhibiting a broader molecular weight distribution, were prepared. First, a base-catalyzed ring-opening polymerization of ε-caprolactone was conducted using a mono-methyl oligo(ethylene glycol) (M_n = 750 Da) as macroinitiator. 1,5,7-Triazabicyclo[4.4.0]dec-5-ene (TBD) was utilized as organo-catalyst in 0.5 mol% relative to the monomer according to a procedure of Hedrick, Waymouth and coworkers.[47] All chemicals were dried carefully prior to usage to suppress unwanted side products due to hydrolyzation of the ester groups or initiation by water. Furthermore, to prevent intra-molecular backbiting or intermolecular chain transfer, increased monomer to initiator ([M]$_0$/[I]$_0$) values were used to reduce the reaction time and thus keeping the dispersity at a

Fig. 1 Comparison of 400 MHz ^{1}H NMR spectra of the monomethyl hexadeca(ethylene glycol) **HO(EG)$_{16}$OMe**, the carboxyl-terminated hexadeca (ε-caprolactone) **TBDMS(CL)$_{16}$CO$_2$H** and the corresponding product *i*-**TBDMS(CL)$_{16}$-(EG)$_{16}$OMe**. Signal **3** of the mOEG$_{16}$ is shifted upfield from 3.59 to 4.22 ppm due to the esterification. All other signals remain at the same chemical shift. These spectra are representative for the synthesis of all three BCP. A full characterization for each of them is provided in the ESI.†

relatively low value. Since we aimed for BCOs similar in M_n compared to *i*-TBDMS(CL)$_n$-(EG)$_{16}$OMe (n = 16, 32, 64) and therefore the same retention time in SEC (assuming a symmetric peak shape), reaction monitoring *via* SEC was performed. Five different approaches, varying in their [M]$_0$/[I]$_0$ values, ranging from [M]$_0$/[I]$_0$ = 40–1226 were performed. A linear relationship of the molecular weight depending on the reaction time was observed for all reactions, whereas the dispersity remained constant ($Đ$ < 1.08) up to a reaction time of three hours. Afterwards, a slight increase was recorded as caused by the already mentioned side reactions (see ESI Table 14 and Fig. 111†). To prevent post-polymerization transesterification, the catalyst was quenched with benzoic acid after the respective reaction time. The most promising results were achieved with [M]$_0$/[I]$_0$ = 167 and 52 min (*p*-TBDMS(CL)$_{17}$-(EG)$_{17}$OMe) as reference for *i*-TBDMS(CL)$_{16}$-(EG)$_{16}$OMe, [M]$_0$/[I]$_0$ = 335 and 109 min (*p*-TBDMS(CL)$_{34}$-(EG)$_{17}$OMe) for *i*-TBDMS(CL)$_{32}$-(EG)$_{16}$OMe, and [M]$_0$/[I]$_0$ = 1226 and 225 min (*p*-TBDMS(CL)$_{74}$-(EG)$_{17}$OMe) for *i*-TBDMS(CL)$_{64}$-(EG)$_{16}$OMe. Unfortunately, the formation of a high molecular weight shoulder, as well as a tailing towards higher retention times *via* mentioned side reactions for *p*-TBDMS(CL)$_{74}$-(EG)$_{17}$OMe could not be suppressed completely or separated *via* silica column chromatography. In order to have similar structures to the uniform BCOs, the alcohol end-group was subsequently converted into the TBDMS ether. An excess of TBDMS-Cl was used to guarantee quantitative protection, which was confirmed by NMR spectroscopy and SEC (see ESI†). The resulting products were purified *via* precipitation, washing and afterwards twice by column chromatography, yielding narrow distributed block cooligomers (*p*-TBDMS(CL)$_n$-(EG)$_{17}$OMe, n = 17, 34, 74), varying in the domain size of the OCL block. Similar retention times and thus M_n values were obtained from SEC analysis for the three BCO pairs (see Fig. 2), which is important for the following comparison.

To investigate the dispersity-dependent structure–property-relationship in terms of the self-assembly behavior of the presented BCOs, differential scanning calorimetry (DSC) and small-angle X-ray scattering (SAXS) analyses were conducted. The corresponding DSC graphs of the BCO pairs of similar size (uniform (red traces) and non-uniform (blue traces)) are individually compared in Fig. 3a–c. Thermal properties and potential differences in thermal transitions were analyzed using the following heating program with two identical cycles: heating from −15 °C to 70 °C at 20 °C min^{-1} and subsequent cooling from 70 °C to −15 °C at −10 °C min^{-1}. A general trend of an increase in both the melting temperature, T_m, and the crystallization temperature, T_c, with increasing degree of polymerization, N, of the OCL block was observed, which are summarized in Table 1.

For the samples *i*-TBDMS(CL)$_{16}$-(EG)$_{16}$OMe and *p*-TBDMS(CL)$_{17}$-(EG)$_{17}$OMe, two melting points were observed for both oligomer samples, with the non-uniform showing two distinct T_ms, whereas for the uniform sample a shoulder towards higher temperatures was observed. A clear trend of a decrease in ΔT_m of the two melting points with increasing N_{OCL} was
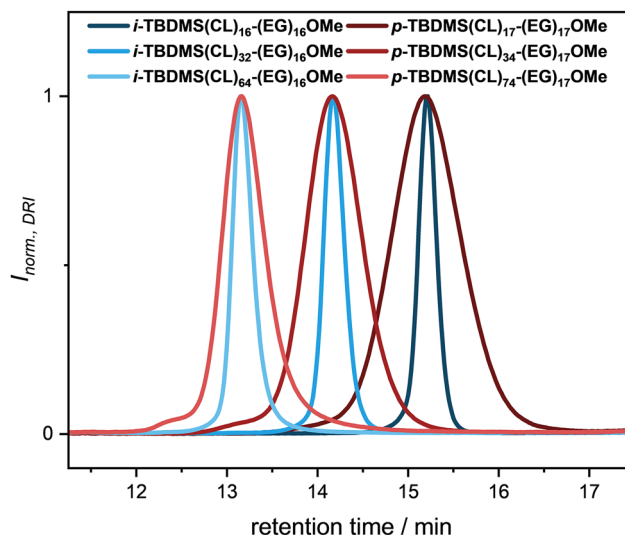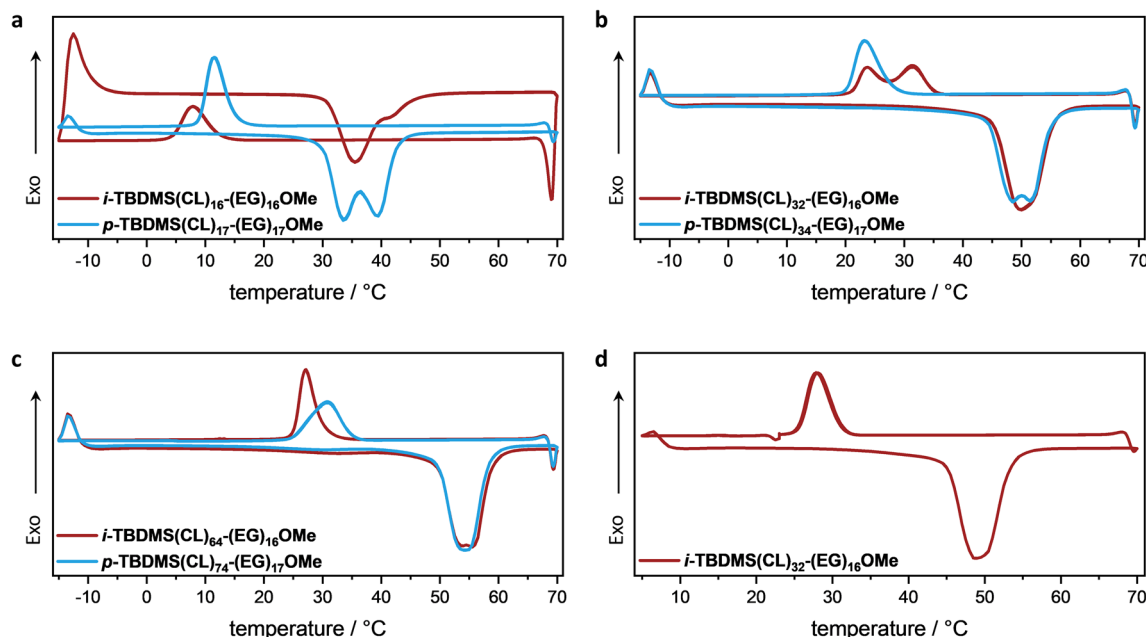

Fig. 2 Comparison of the SEC traces of the three uniform BCOs (*i*-TBDMS(CL)$_n$-(EG)$_{16}$OMe, n = 16, 32, 64, blue) prepared *via* an iterative synthesis strategy and the corresponding disperse (*p*-TBDMS(CL)$_n$-(EG)$_{17}$OMe, n = 17, 34, 74, red) BCOs obtained from ROP of ε-caprolactone.

observed for the non-uniform samples. For *p*-TBDMS(CL)$_{17}$-(EG)$_{17}$OMe, a difference of ΔT_m = 6 °C and 3 °C for *p*-TBDMS(CL)$_{34}$-(EG)$_{17}$OMe were observed, whereas *p*-TBDMS(CL)$_{74}$-(EG)$_{17}$OMe showed only one melting temperature at 54 °C. In comparison, for the uniform BCOs with N_{OCL} = 32 and N_{OCL} = 64, only one melting transition at 48 °C and 55 °C was observed, respectively. For the crystallization transition, a shift towards lower temperatures was observed with decreasing temperature for the samples *i*-TBDMS(CL)$_{16}$-(EG)$_{16}$OMe and *i*-TBDMS(CL)$_{64}$-(EG)$_{16}$OMe compared to the corresponding non-uniform BCOs (*p*-TBDMS(CL)$_{17}$-(EG)$_{17}$OMe and *p*-TBDMS(CL)$_{74}$-(EG)$_{17}$OMe). This behavior could be explained by larger macromolecules only present within the non-uniform samples, which could act as crystallization nuclei. Interestingly, the uniform BCP with N_{OCL} = 32 (*i*-TBDMS(CL)$_{32}$-(EG)$_{16}$OMe) showed two crystallization transitions at T_c = 24 °C and T_c = 32 °C, whereas only one transition at T_c = 24 °C was observed for the corresponding non-uniform sample (*p*-TBDMS(CL)$_{34}$-(EG)$_{17}$OMe). To slow down the crystallization process, the temperature program was adjusted by inserting an isotherm for 5 min at 23 °C (Fig. 3d). Thus, only a single crystallization transition was observed for *i*-TBDMS(CL)$_{32}$-(EG)$_{16}$OMe, indicating the crystallization being slower than the initial cooling rate. Furthermore, no noticeable difference in the comparison of the melting enthalpy, ΔH_m, of the uniform and non-uniform samples with N_{OCL} = 32 and N_{OCL} = 64 (see Table 1, please note: for *i*-TBDMS(CL)$_{16}$-(EG)$_{16}$OMe an exothermic phase transition was observed at −13 °C in the heating cycle. Therefore, these results were not considered in the comparison) were observed.

For investigations of the long-range-order distance and to observe first insights into the morphology of the BCOs, SAXS

Fig. 3 DSC traces of the individual uniform (red) and non-uniform (blue) BCO pairs (a–c) using a heating program with two identical cycles: heating from −15 °C to 70 °C at 20 °C min^{-1} and subsequent cooling from 70 °C to −15 °C at −10 °C min^{-1}. (d) DSC trace of i-TBDMS(CL)$_{32}$-(EG)$_{16}$OMe using a heating program as follows: 5 °C to 70 °C at 20 °C min^{-1} and subsequent cooling from 70 °C to 23 °C at −10 °C min^{-1}, keeping that temperature for 5 min; cooling from 23 °C to 5 °C at −10 °C min^{-1}.

Table 1 Comparison of DSC results of the uniform and non-uniform BCOs

Sample	m/mg	T_c^{onset}/°C	T_c^{peak}/°C	ΔH_c /J g^{-1}	T_m^{onset}/°C	T_m^{peak}/°C	ΔH_m/J g^{-1}
i-TBDMS(CL)$_{16}$-(EG)$_{16}$OMe	5.3	13	8	36	31	35	−38
p-TBDMS(CL)$_{17}$-(EG)$_{17}$OMe	5.3	15	12	56	30	34/40	−58
i-TBDMS(CL)$_{32}$-(EG)$_{16}$OMe	6.5	28	24/32	60	44	48	−63
p-TBDMS(CL)$_{34}$-(EG)$_{17}$OMe	6.5	30	24	60	45	49/52	−63
i-TBDMS(CL)$_{64}$-(EG)$_{16}$OMe	5.5	30	28	58	49	55	−57
p-TBDMS(CL)$_{74}$-(EG)$_{17}$OMe	5.5	35	31	57	49	54	−55

analysis was performed. In this context, the uniform and non-uniform BCOs (i-TBDMS(CL)$_n$-(EG)$_{16}$OMe, n = 16, 32, 64 and p-TBDMS(CL)$_n$-(EG)$_{17}$OMe, n = 17, 34, 74) were self-assembled directly on Kapton® foil via either thermal or solvent vapor annealing (SVA) with acetone. For thermal annealing, the sample was heated to 70 °C (21–40 °C above T_m^{onset}) under vacuum, kept at that temperature for three hours and was subsequently cooled to room temperature overnight. To evaluate the long-range-order distance (domain size, $L_0 = 2\pi/q_0$) in the uniform and non-uniform BCOs, SAXS was performed at room temperature. The 1D SAXS patterns for the thermally annealed samples are shown in Fig. 4a–c. In general, the samples show SAXS reflections at $1q_0$ and $3q_0$ consistent with a symmetric lamellar morphology, except for i-TBDMS(CL)$_{16}$-(EG)$_{16}$OMe$_{therm}$. (Fig. 4a, red trace), which had an exact degree of polymerization of N = 16 for both the OEG and OCL block, that lacked the higher-order peak. Compared to the corresponding non-uniform BCO (p-TBDMS(CL)$_{17}$-(EG)$_{17}$OMe$_{therm.}$, Fig. 4a, blue trace), a single broad peak at q_0 = 0.42 Å^{-1} was observed indicating a less ordered structure. These obser-

vations are inconsistent with the findings of Meijer and Palmans $et\ al.$ as well as with Hawker, Bates and coworkers, who describe the opposite effect for uniform and non-uniform oligo(DMS-b-LA) BCPs[13] and oligo(DMS-b-MMA) BCPs,[15] respectively. With a decrease in dispersity, an increase in the (long-range) order was described.[13,15] On the other hand, note that the reported difference in dispersity of the compared BCPs is twice as large ($\Delta Đ \sim 0.13$)[15] as for the BCOs described herein ($\Delta Đ = 0.05$). i-TBDMS(CL)$_{16}$-(EG)$_{16}$OMe and p-TBDMS(CL)$_{17}$-(EG)$_{17}$OMe are similar in their volume fraction of OCL ($\Phi_{OCL} = 0.71$), but the latter BCO contains longer-chain oligomers, which might form an ordered state due to a higher χN value and could thus be decisive for the effect in segregation.

Similar results for the degree of order, as described for the thermal annealing of i-TBDMS(CL)$_{16}$-(EG)$_{16}$OMe and p-TBDMS(CL)$_{17}$-(EG)$_{17}$OMe, were observed for the self-assembly via SVA in acetone (Fig. 4d). Due to the less pronounced phase separation, a broader peak was observed at q_0 = 0.59 Å^{-1} (Fig. 4a), corresponding to a decrease in the long-range-order distance of ΔL_0 = 3.1 nm ($L_0(i$-TBDMS(CL)$_{16}$-(EG)$_{16}$OMe$_{SVA}$) = 10.5 nm)
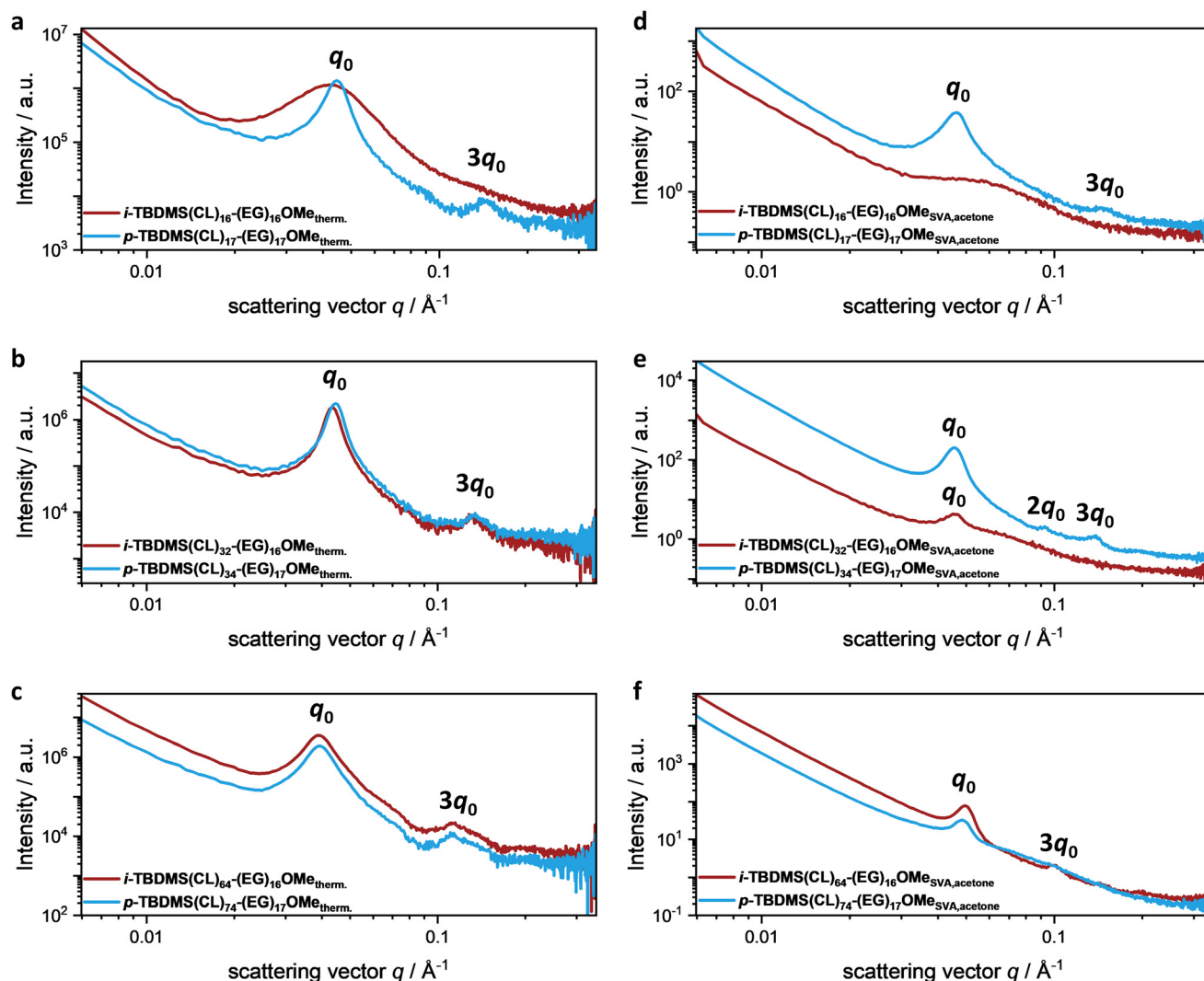
Fig. 4 : SAXS data for the uniform (i-TBDMS(CL)$_n$-(EG)$_{16}$OMe, n = 16, 32, 64, red traces) and non-uniform BCP (p-TBDMS(CL)$_n$-(EG)$_{17}$OMe, n = 17, 34, 74, blue traces). Self-assembly *via* thermal (a–c) or solvent vapor (d–f) annealing on Kapton® foil.

compared to the non-uniform p-**TBDMS(CL)$_{17}$-(EG)$_{17}$OMe** (L_0(p-**TBDMS(CL)$_{17}$-(EG)$_{17}$OMe$_{SVA}$**) = 13.6 nm). A similar trend is observed for i-**TBDMS(CL)$_{32}$-(EG)$_{16}$OMe$_{SVA}$** (L_0 = 13.6 nm), and p-**TBDMS(CL)$_{34}$-(EG)$_{17}$OMe$_{SVA}$** (L_0 = 13.8 nm) (ΔL_0 = 0.2 nm, Fig. 4e) as well as i-**TBDMS(CL)$_{64}$-(EG)$_{16}$OMe$_{SVA}$** (L_0 = 12.6 nm) and p-**TBDMS(CL)$_{74}$-(EG)$_{17}$OMe$_{SVA}$** (L_0 = 13.0 nm) with a difference of L_0 = 0.4 nm (Fig. 4f).

Thus, even small differences of $\Delta Đ = 0.05$ in relation to the uniform BCOs affected the expansion of the lamellar period for the SVA, resulting in an increase of the primary Bragg reflection q_0, which is in agreement with the results of previous experimental reports and predictions by self-consistent field theory (SCFT).[10,13,15]

However, a contradictory trend was obtained for the samples self-assembled *via* thermal annealing (Fig. 4a–c). A decrease in the dispersity resulted in an increase of the L_0 up to 4% (0.5 nm for N = 32) compared to the non-uniform BCPs. Since the scattering vector, q_0, is proportional to the radius of

gyration, R_g, which in turn is proportional to $N^{2/3}$ (assuming lamellar morphologies), shorter chains in a non-uniform oligomer have greater impact on R_g. Thus, smaller values for q_0 are expected for a symmetrical widening of the molecular weight distribution, resulting in larger L_0 (Table 2, thermal). Similar results were reported by Fors *et al.* for truly dispersed polymers showing a positively and negatively skewed molecular weight distribution.[16] Furthermore, an increase of Φ_{OCL} resulted in an expected increase in L_0 for the thermal annealing (excluding the less ordered i-**TBDMS(CL)$_{16}$-(EG)$_{16}$OMe$_{therm}$**), where an inverted trend was observed for the SVA of the samples in acetone.

In summary, a clear difference in the self-assembly behavior of the uniform and non-uniform OCL-OEG BCOs with Φ_{OCL} = 0.71 was demonstrated for thermal as well as solvent vapor annealing. Furthermore, an increase of the long-range-order distance L_0 with increasing dispersity was obtained for all BCOs *via* SVA, which is in accordance with the literature.

Table 2 Primary SAXS peak analysis for the uniform (*i*-TBDMS(CL)$_n$-(EG)$_{16}$OMe, n = 16, 32, 64) and non-uniform (*p*-TBDMS(CL)$_n$-(EG)$_{16}$OMe, n = 17, 34, 74) BCOs

Sample	N_{OEG}	N_{CL}	$Đ^a$	$Φ_{OCL}{}^c$	$L_0{}^d$/nm	$L_0{}^e$/nm
i-**TBDMS(CL)$_{16}$-(EG)$_{16}$OMe**	16	16	1.01	0.71	14.8	10.5
i-**TBDMS(CL)$_{32}$-(EG)$_{16}$OMe**	16	32	1.01	0.83	14.6	13.6
i-**TBDMS(CL)$_{64}$-(EG)$_{16}$OMe**	16	64	1.01	0.91	16.1	12.6
p-**TBDMS(CL)$_{17}$-(EG)$_{17}$OMe**	17^a	17^b	1.06	0.71	14.1	13.6
p-**TBDMS(CL)$_{34}$-(EG)$_{17}$OMe**	17^a	34^b	1.06	0.83	14.1	13.8
p-**TBDMS(CL)$_{74}$-(EG)$_{17}$OMe**	17^a	74^b	1.06	0.92	15.8	13.0

^{a} Determined *via* SEC (system III). ^{b} Determined *via* ^{1}H NMR. ^{c} OCL volume fraction using densities of 1.094 g mL^{-1} for mOEG (M_n = 750 Da) and 1.146 g mL^{-1} for PCL (average M_w ~ 14k; average M_n ~ 10k by SEC). ^{d} Long-range order distance calculated *via* $L_0 = 2\pi/q_0$ (thermal annealing). ^{e} Long-range order distance calculated *via* $L_0 = 2\pi/q_0$ (solvent vapor annealing).

Contradictory results were obtained for both annealing processes and no expected narrowing of the signals was observed. However, differences in solvent and thermal annealing are a literature-known phenomenon.[48]

Conclusion

We describe the synthesis of uniform OCL-OEG block cooligomers *via* a Steglich esterification of the corresponding OEG and OCL homooligomers, which were prepared *via* an iterative exponential growth strategy. A OCL containing 64 repeating units was obtained in 20 steps in an overall yield of 33% according to the optimized reaction protocol of Hawker *et al.*[41] TBDMS ether and benzyl ester were employed as orthogonal protecting groups. Consistently high yields for both the deprotection (>95%) and the coupling steps (>83%) were achieved. For the synthesis of uniform OEGs, THP and benzyl ether as protecting groups and KO^{t}Bu as base for the etherification showed the most promising results and a uniform mOEG$_{16}$ was obtained in 11 steps in an overall yield of 3%. Three uniform OCL-OEG BCOs ($Đ$ = 1.01), varying in the length of the OCL domain, were synthesized. Identical structures, similar in M_n with the uniform BCO, but exhibiting a slightly broader molecular weight distribution ($Đ$ = 1.06) were prepared *via* ROP of ε-caprolactone and the influence of the dispersity on thermal properties and morphologies obtained *via* self-assembly through thermal and solvent-vapor annealing was investigated by DSC and SAXS analysis, respectively. Significantly increased crystallization temperatures, T_c, were observed for *p*-**TBDMS-(CL)$_{17}$-(EG)$_{17}$OMe** and *p*-**TBDMS-(CL)$_{34}$-(EG)$_{17}$OMe** in comparison with their uniform analogues. Furthermore, SAXS analysis revealed an increase in the long-range order distance, L_0, and a less pronounced phase separation for *i*-**TBDMS(CL)$_{16}$-(EG)$_{16}$OMe**, with a decrease in dispersity of the BCOs.

Data availability

The datasets supporting this article have been uploaded as part of the ESI.†

Conflicts of interest

The authors declare no conflict of interests.

Acknowledgements

References

1 (*a*) Y. Mai and A. Eisenberg, *Chem. Soc. Rev.*, 2012, **41**, 5969; (*b*) S. B. Darling, *Prog. Polym. Sci.*, 2007, **32**, 1152; (*c*) A. Blanazs, S. P. Armes and A. J. Ryan, *Macromol. Rapid Commun.*, 2009, **30**, 267.

2 P. Alexandridis and B. Lindman, *Amphiphilic block copolymers. Self-assembly and applications*, Elsevier, Amsterdam, 1st edn, 2000.

3 A. Rösler, G. W. Vandermeulen and H.-A. Klok, *Adv. Drug Delivery Rev.*, 2012, **64**, 270.

4 R. A. Segalman, B. McCulloch, S. Kirmayer and J. J. Urban, *Macromolecules*, 2009, **42**, 9205.

5 H.-A. Klok and S. Lecommandoux, *Adv. Mater.*, 2001, **13**, 1217.

6 (*a*) M. L. Huggins, *J. Chem. Phys.*, 1941, **9**, 440; (*b*) P. J. Flory, *J. Chem. Phys.*, 1942, **10**, 51.

7 L. Leibler, *Macromolecules*, 1980, **13**, 1602.

8 (*a*) F. S. Bates and G. H. Fredrickson, *Phys. Today*, 1999, **52**, 32; (*b*) S. Förster and T. Plantenberg, *Angew. Chem., Int. Ed.*, 2002, **41**, 688; (*c*) J. K. Kim, S. Y. Yang, Y. Lee and Y. Kim, *Prog. Polym. Sci.*, 2010, **35**, 1325; (*d*) M. C. Orilall and U. Wiesner, *Chem. Soc. Rev.*, 2011, **40**, 520.

9 (*a*) J. C. van Hest, D. A. Delnoye, M. W. Baars, M. H. van Genderen and E. W. Meijer, *Science*, 1995, **268**, 1592; (*b*) L. Zhang, K. Yu and A. Eisenberg, *Science*, 1996, **272**, 1777; (*c*) L. Zhang and A. Eisenberg, *Science*, 1995, **268**, 1728.

10 N. A. Lynd and M. A. Hillmyer, *Macromolecules*, 2005, **38**, 8803.

11 (*a*) K. E. B. Doncom, L. D. Blackman, D. B. Wright, M. I. Gibson and R. K. O'Reilly, *Chem. Soc. Rev.*, 2017, **46**, 4119; (*b*) O. Terreau, L. Luo and A. Eisenberg, *Langmuir*, 2003, **19**, 5601; (*c*) S. R. George, R. Champagne-Hartley, G. A. Deeter, J. D. Campbell, B. Reck, D. Urban and M. F. Cunningham, *Macromolecules*, 2017, **50**, 315; (*d*) Y. Hirai, T. Terashima, M. Takenaka and M. Sawamoto, *Macromolecules*, 2016, **49**, 5084; (*e*) A. Buckinx, M. Rubens, N. R. Cameron, C. Bakkali-Hassani, A. Sokolova and T. Junkers, *Polym. Chem.*, 2022, **13**, 3444; (*f*) E. Konishcheva, D. Häussinger, S. Lörcher and W. Meier, *Eur. Polym. J.*, 2016, **83**, 300; (*g*) Y. Jiang, M. R. Golder, H. V.-T. Nguyen,

Y. Wang, M. Zhong, J. C. Barnes, D. J. C. Ehrlich and J. A. Johnson, *J. Am. Chem. Soc.*, 2016, **138**, 9369; (*h*) M. R. Golder, Y. Jiang, P. E. Teichen, H. V.-T. Nguyen, W. Wang, N. Milos, S. A. Freedman, A. P. Willard and J. A. Johnson, *J. Am. Chem. Soc.*, 2018, **140**, 1596.

12 B. van Genabeek, B. F. M. de Waal, M. M. J. Gosens, L. M. Pitet, A. R. A. Palmans and E. W. Meijer, *J. Am. Chem. Soc.*, 2016, **138**, 4210.

13 B. van Genabeek, B. F. M. de Waal, B. Ligt, A. R. A. Palmans and E. W. Meijer, *ACS Macro Lett.*, 2017, **6**, 674.

14 C. Zhang, M. W. Bates, Z. Geng, A. E. Levi, D. Vigil, S. M. Barbon, T. Loman, K. T. Delaney, G. H. Fredrickson, C. M. Bates, A. K. Whittaker and C. J. Hawker, *J. Am. Chem. Soc.*, 2020, **142**, 9843.

15 B. Oschmann, J. Lawrence, M. W. Schulze, J. M. Ren, A. Anastasaki, Y. Luo, M. D. Nothling, C. W. Pester, K. T. Delaney, L. A. Connal, A. J. McGrath, P. G. Clark, C. M. Bates and C. J. Hawker, *ACS Macro Lett.*, 2017, **6**, 668.

16 D. T. Gentekos, J. Jia, E. S. Tirado, K. P. Barteau, D.-M. Smilgies, R. A. DiStasio and B. P. Fors, *J. Am. Chem. Soc.*, 2018, **140**, 4639.

17 D. T. Gentekos and B. P. Fors, *ACS Macro Lett.*, 2018, **7**, 677.

18 D. T. Gentekos, R. J. Sifri and B. P. Fors, *Nat. Rev. Mater.*, 2019, **4**, 761.

19 J.-F. Lutz, *Polym. Chem.*, 2010, **1**, 55.

20 J.-F. Lutz, M. Ouchi, D. R. Liu and M. Sawamoto, *Science*, 2013, **341**, 1238149.

21 (*a*) P. Nanjan and M. Porel, *Polym. Chem.*, 2019, **10**, 5406; (*b*) M. A. R. Meier and C. Barner-Kowollik, *Adv. Mater.*, 2019, **31**, e1806027; (*c*) S. A. Hill, C. Gerke and L. Hartmann, *Chem. – Asian J.*, 2018, **13**, 3611; (*d*) R. Aksakal, C. Mertens, M. Soete, N. Badi and F. Du Prez, *Adv. Sci.*, 2021, **8**, 2004038; (*e*) A. S. Knight, E. Y. Zhou, M. B. Francis and R. N. Zuckermann, *Adv. Mater.*, 2015, **27**, 5665; (*f*) Z. Deng, Q. Shi, J. Tan, J. Hu and S. Liu, *ACS Mater. Lett.*, 2021, **3**, 1339.

22 S. C. Solleder, R. V. Schneider, K. S. Wetzel, A. C. Boukis and M. A. R. Meier, *Macromol. Rapid Commun.*, 2017, **38**, 1600711.

23 R. B. Merrifield, *J. Am. Chem. Soc.*, 1963, **85**, 2149.

24 R. B. Merrifield, *Angew. Chem., Int. Ed. Engl.*, 1985, **24**, 799.

25 R. J. Simon, R. S. Kania, R. N. Zuckermann, V. D. Huebner, D. A. Jewell, S. Banville, S. Ng, L. Wang, S. Rosenberg and C. K. Marlowe, *Proc. Natl. Acad. Sci. U. S. A.*, 1992, **89**, 9367.

26 H. Herzner, T. Reipen, M. Schultz and H. Kunz, *Chem. Rev.*, 2000, **100**, 4495.

27 S. L. Beaucage and M. H. Caruthers, *Tetrahedron Lett.*, 1981, **22**, 1859.

28 B. Genabeek, B. A. G. Lamers, C. J. Hawker, E. W. Meijer, W. R. Gutekunst and B. V. K. J. Schmidt, *J. Polym. Sci.*, 2021, **59**, 373.

29 (*a*) J. W. Grate, K.-F. Mo and M. D. Daily, *Angew. Chem.*, 2016, **128**, 3993; (*b*) A. Al Ouahabi, M. Kotera, L. Charles and J.-F. Lutz, *ACS Macro Lett.*, 2015, **4**, 1077; (*c*) S. Martens, J. van den Begin, A. Madder, F. E. Du Prez and P. Espeel, *J. Am. Chem. Soc.*, 2016, **138**, 14182.

30 (*a*) W. Konrad, C. Fengler, S. Putwa and C. Barner-Kowollik, *Angew. Chem., Int. Ed.*, 2019, **58**, 7133; (*b*) J. C. Barnes, D. J. C. Ehrlich, A. X. Gao, F. A. Leibfarth, Y. Jiang, E. Zhou, T. F. Jamison and J. A. Johnson, *Nat. Chem.*, 2015, **7**, 810.

31 X. Tong, B. Guo and Y. Huang, *ChemComm*, 2011, **47**, 1455.

32 J. J. Haven, J. A. de Neve and T. Junkers, *ACS Macro Lett.*, 2017, **6**, 743.

33 (*a*) S. Ida, T. Terashima, M. Ouchi and M. Sawamoto, *J. Am. Chem. Soc.*, 2009, **131**, 10808; (*b*) S. Ida, M. Ouchi and M. Sawamoto, *Macromol. Rapid Commun.*, 2011, **32**, 209.

34 (*a*) O. I. Paynter, D. J. Simmonds and M. C. Whiting, *J. Chem. Soc., Chem. Commun.*, 1982, 1165; (*b*) G. M. Brooke, S. Burnett, S. Mohammed, D. Proctor and M. C. Whiting, *J. Chem. Soc., Perkin Trans. 1*, 1996, 1635.

35 B. A. G. Lamers, R. Graf, B. F. M. de Waal, G. Vantomme, A. R. A. Palmans and E. W. Meijer, *J. Am. Chem. Soc.*, 2019, **141**, 15456.

36 B. A. G. Lamers, B. P. Fors and E. W. Meijer, *J. Polym. Sci.*, 2022, **61**, 929.

37 Y. Kim, H. Park, A. Abdilla, H. Yun, J. Han, G. E. Stein, C. J. Hawker and B. J. Kim, *Chem. Mater.*, 2020, **32**, 3597.

38 J. Chen, A. Rizvi, J. P. Patterson and C. J. Hawker, *J. Am. Chem. Soc.*, 2022, **144**, 19466.

39 E. A. Murphy, Y.-Q. Chen, K. Albanese, J. R. Blankenship, A. Abdilla, M. W. Bates, C. Zhang, C. M. Bates and C. J. Hawker, *Macromolecules*, 2022, **55**, 8875.

40 Y. Kwon and K. T. Kim, *Macromolecules*, 2021, **54**, 10487.

41 K. Takizawa, C. Tang and C. J. Hawker, *J. Am. Chem. Soc.*, 2008, **130**, 1718.

42 P. Bohn and M. A. R. Meier, *Polym. J.*, 2020, **52**, 165.

43 Q. Zhang, H. Ren and G. L. Baker, *Tetrahedron Lett.*, 2014, **55**, 3384.

44 K. Maranski, Y. G. Andreev and P. G. Bruce, *Angew. Chem., Int. Ed.*, 2014, **53**, 6411.

45 M. Shan, A. Bujotzek, F. Abendroth, A. Wellner, R. Gust, O. Seitz, M. Weber and R. Haag, *ChemBioChem*, 2011, **12**, 2587.

46 V. Gold, in *The IUPAC Compendium of Chemical Terminology*, ed. V. Gold, International Union of Pure and Applied Chemistry (IUPAC), Research Triangle Park, NC, 2019. https://goldbook.iupac.org/terms/view/U06558, (accessed June 2023).

47 B. G. G. Lohmeijer, R. C. Pratt, F. Leibfarth, J. W. Logan, D. A. Long, A. P. Dove, F. Nederberg, J. Choi, C. Wade, R. M. Waymouth and J. L. Hedrick, *Macromolecules*, 2006, **39**, 8574.

48 X. Gu, I. Gunkel, A. Hexemer and T. P. Russell, *Macromolecules*, 2016, **49**, 3373.